VERY HIGH PRECISION ORBIT OF CAPELLA BY LONG BASELINE INTERFEROMETRY

C.A. HUMMEL[1], J.T. ARMSTRONG[1], A. QUIRRENBACH[1], D.F. BUSCHER[1], D. MOZURKEWICH[2], N.M. ELIAS II[3]

NRL/USNO Optical Interferometer Project

U.S. Naval Observatory, 3450 Massachusetts Avenue NW, Washington, DC 20392

R.E. WILSON

211 SSRB, Department of Astronomy, University of Florida, Gainesville, FL 32611

[1]Universities Space Research Association, 300 D St. SW, Suite 801, Washington, DC 20024

[2]Remote Sensing Division, Naval Research Laboratory, Code 7200, Washington, DC 20375

[3]U.S. Naval Observatory, Code AD5, 3450 Massachusetts Ave. NW, Washington, DC 20392

ABSTRACT

The orbital elements of the double-lined spectroscopic binary Capella have been determined with unprecedented accuracy from observations with the Mark III optical interferometer. We have measured a magnitude difference, $m_{\rm Aa} - m_{\rm Ab}$, of $-0\overset{\rm m}{.}05 \pm 0\overset{\rm m}{.}05$, $0\overset{\rm m}{.}15 \pm 0\overset{\rm m}{.}05$, and $0\overset{\rm m}{.}28 \pm 0\overset{\rm m}{.}10$ at $\lambda\lambda$ 800 nm, 550 nm, and 450 nm, respectively. We confirm previous observations that the more massive spectroscopic primary component Aa is also the cooler and visually fainter of the two stars. Measured stellar radii are $R_{\rm Aa} = (12.2 \pm 0.2) R_\odot$ and $R_{\rm Ab} = (9.2 \pm 0.4) R_\odot$. There is some evidence in our data for a departure of the brightness distribution of component Ab from a simple limb-darkened disk, possibly related to star spots. Using spectroscopy by Barlow *et al.* (1993, PASP 105, 476), we derive component masses of $\mathcal{M}_{\rm Aa} = (2.69 \pm 0.06)\ \mathcal{M}_\odot$ and $\mathcal{M}_{\rm Ab} = (2.56 \pm 0.04)\ \mathcal{M}_\odot$. Comparison with recent stellar evolution models (Schaerer *et al.* 1993, A&AS, 98, 523) yields a stellar age of $5.25 \cdot 10^8$ yrs for a metallicity of $Z = 0.008$. In this scenario, component Aa has undergone helium ignition.

1. INTRODUCTION

Capella has acquired the reputation of an ideal target for various interferometric methods ever since the first of such observations were performed by Anderson (1920) and Merrill (1922), who mounted a Michelson interferometer on top of the Mt. Wilson 100-inch reflector and resolved the ≈ 60 milliarcsecond (mas) angular separation between the two components. From measurements of separation and position angle at several epochs, Anderson and Merrill derived the orbital elements of the system with a precision not to be exceeded until the advent of long-baseline interferometry several decades later. Meanwhile, speckle interferometric techniques were developed and have been used by McAlister (1981) and Bagnuolo & Hartkopf (1989) to derive recent elements, and by Bagnuolo & Sowell (1988) to determine the small but nevertheless significant brightness difference between the components. Di Benedetto and Bonneau (1991) then used a long-baseline infrared interferometer to measure the size of one the two stars of Capella.

Observations of the double-lined spectrum of Capella resulted in the identification of a hotter component (Ab) of spectral type G1III and a cooler component (Aa) of type G8III or K0III (Strassmeier & Fekel 1990). Spectroscopic observations are complicated by the fact that the lines of the hotter component are rotationally broadened ($v \sin i = 36 \pm 3$ km/s: Fekel *et al.* 1986, Griffin & Griffin 1986). Therefore, this component has carried other classifications in the past, e.g. G0III (Wright 1954), or F9III (Ayres & Linsky 1980). It follows, with an estimate for the diameter of 9.2 $R_\odot$ (see discussion), that the hot component completes about 12 revolutions in one orbital period of 104 days. Griffin & Griffin (1986) were the first to show that the hotter component is the brighter one by $0\overset{\mathrm{m}}{.}15$ in visual light, a result subsequently confirmed by Bagnuolo & Sowell (1988). We will follow common practice in calling the visually brighter component (the spectroscopic secondary) component Ab and the other component Aa.

Capella (= α Aurigae = 13 Aurigae = HR 1708 = HD 34029 = SAO 40186 = FK5 193 = No. 306 in the catalog by Batten *et al.* [1989], $\alpha = 5^{\mathrm{h}}16^{\mathrm{m}}41.4^{\mathrm{s}}$, $\delta = 45°59'53''$

[epoch 2000.0], $m_V = 0\overset{\mathrm{m}}{.}08$), is the brightest member of ADS 3841. All other components are faint ($m_V > 10^{\mathrm{m}}$) and distant ($> 12'$) (Hoffleit & Jaschek 1982). There is indication of enhanced activity in this system. Hall (1981) included Capella in his list of RS CVn stars with a variability amplitude of $0\overset{\mathrm{m}}{.}15$. The star is also listed with a similar variability amplitude in the catalogs by Kukarkin *et al.* (1982) and Petit (1990). However, Krisciunas & Guinan (1990) reported an upper limit of $0\overset{\mathrm{m}}{.}04$ for the variability amplitude of Capella based on measurements from 1981 to 1990. Chromospheric activity noted in Capella was traced to component Ab by Ayres & Linsky (1980), thus indicating that the rotation of this component is the common origin of enhanced activity.

The observations reported in this paper were obtained with the Mark III interferometer[4] as part of a program aimed at the resolution and determination of the orbits of spectroscopic binaries with angular sizes on the order of a few mas (for a recent summary of results see Hummel & Armstrong 1993). In particular, we recognized the need to demonstrate our methods with a very well known binary orbit, as is the orbit of Capella today.

2. OBSERVATIONS AND DATA REDUCTION

The Mark III interferometer (Shao *et al.* 1988) combines the light of two apertures, which can be positioned between 3 m and 31 m apart, in order to produce a stellar interference ("fringe") pattern. Its contrast, the visibility contains spatial information on the object. The geometric delay is compensated for in vacuum, so that first order atmospheric refraction effects are negligible. The data were obtained during 38 nights in autumn and winter of the years between 1988 and 1992 (mean epoch and equinox JD 2448592 = 1991.9). We measured the visibility of Capella in narrowband channels covering the red, green, and blue portion of the spectrum by comparison with the visibility

[4]The Mark III Long-Baseline Optical Interferometer located on Mt. Wilson near Los Angeles, California, is operated by the Remote Sensing Division of the Naval Research Laboratory (NRL) with funding from the Office of Naval Research.

of unresolved calibrator stars. (An ideal interferometer measures a visibility of unity on unresolved stars.) Observations were switched between Capella and other program and calibrator stars throughout the night. We used the north-south baselines of the Mark III interferometer with lengths ranging from 3.0 m to 23.6 m, as well as the northeast-southwest baseline with a fixed length of 12.0 m.

The Mark III interferometer coherently averages the fringe pattern in each of the four available channels for 4 ms and uses its phase in a broadband channel (650 nm – 900 nm) as an error signal to track the rapid fringe motion induced by atmospheric turbulence. An estimator for the square of the visibility, V^2, is calculated offline, integrated incoherently to 0.5 s, edited, further averaged to a scan of 75 seconds, and corrected for the background count. Only data from the narrow channels are used for further analysis, since the visibility degradation, when the Mark III tracks one or two fringes off the central fringe, is negligible only for small bandwidths.

The calibration of the data, i.e. the normalization of the visibility of the program stars by the visibility of the calibrators, follows the procedures described in detail by Armstrong *et al.* (1992) and Mozurkewich *et al.* (1991). Essentially, the visibility of the calibrator scans is used to establish the functional dependence of the normalization factor on the seeing index, zenith angle, angle of incidence on the siderostat mirror, and time. (The seeing index is a measure of the strength of the atmospheric fluctuations. The dependence of the visibility on the seeing index is usually the dominant effect.) Diameters (and hence the visibilities) of the calibrators were estimated from their apparent visual magnitudes and the $(R - I)$ color indices with a procedure given by Mozurkewich *et al.* (1991). Except for α Persei (uniform disk diameter of 3.0 mas), we chose calibrators with estimated diameters smaller than about 1.5 mas, resulting in estimated squared visibilities larger than 80 per cent on any baseline. A calibration uncertainty, to be added to the photon-noise-induced variance of the visibilities in quadrature, was estimated so as to result in a reduced χ^2, denoted χ^2_ν, of unity for the fit of the calibrator visibilities to their

estimated values. Calibration uncertainties are typically a few percent for the red channel and up to 15 per cent for the blue channel. In Fig. 1 we show the error distribution of the calibrators in the red, green, and blue channels, as well as the total distribution including data of all channels. Errors are defined as the deviation of the measured (calibrated) visibilities from the model (estimated) visibilities, divided by the formal uncertainties of the measured visibilities. The shapes of the distributions are very close to a Gaussian for a reduced χ^2 of unity.

Figure 2 shows a sample of (squared) visibilities for Capella, measured November 13, 1991, on a north-south baseline of 11.4-m length. Due to earth rotation, the baseline vector passes through the loci of maxima and minima of the visibility function of the binary. The separation of the components in that night was 55.2 mas at a position angle of 27°.3. The visibility was measured through filters centered at $\lambda\lambda$ 801.3 nm, 548.3 nm, and 501.3 nm. In other nights, we used combinations of these filters and filters centered at $\lambda\lambda$ 656.6 nm, 657.0 nm, 499.5 nm, and 450.0 nm. (The two filters centered on the Hα line were installed when Capella was observed together with a list of Be stars. No peculiar effects were noticed in these bands.) Filter bandwidths range from 1 nm to 40 nm. In addition to the factory specifications, we obtained measurements of the transmission curves for all filters (except the one at λ 450 nm) in order to calibrate bandpasses and central wavelengths to better than $\pm$0.5 nm.

3. ESTIMATION OF COMPONENT PARAMETERS AND ORBITAL ELEMENTS

We used the method introduced by Hummel *et al.* (1993) to fit orbital elements and component parameters directly to the visibilities, rather than fitting the orbit to separation ρ and position angle θ of the binary determined from the data of individual nights. The seven orbital elements are the major axis a in mas, eccentricity e, period P, epoch of periastron passage T, inclination i, position angle of the ascending node Ω, and the argument of the periastron ω. Component parameters are the diameters $D_{1,2}$ and magnitude differences $\Delta m(\lambda)$ of the components at $\lambda\lambda$ 800 nm, 550 nm, and

450 nm (approximately corresponding to bands I_C, V, and B, respectively). Values of the component parameters at other observed wavelengths are interpolated by quadratic polynomials. This 'global' fit is the most efficient approach to constrain the component parameters if the components are not significantly variable. The method can also make use of data taken on nights with insufficient coverage to constrain a fit of ρ and θ, and is able to derive orbital elements when the orbital motion is too large to define ρ and θ uniquely for a single night.

We adopted circularly symmetric disks with linear limb darkening for the components. The limb-darkening coefficients $A_{1,2}$ (see Table 4) were obtained from tables by Manduca (1979) and Manduca *et al.* (1977) for the model ($T_{\rm eff}$ = 6000 K, $\log g$ = 3.0, $[A/H]$=0) for component Ab, and for the model ($T_{\rm eff}$ = 5000 K, $\log g$ = 3.0, $[A/H]$=0) for Aa. The model visibilities of a limb-darkened disk were calculated with the formula given by Hanbury Brown *et al.* (1974) and by integration over the filter bandpass weighted with the stellar flux distribution (adopting a black body spectrum). Both components of Capella are easily resolved on the longer baselines. This can be seen in Fig. 3, as the upper envelope of the measured visibilities drops with increasing baseline length.

Orbital elements derived from speckle interferometric observations provided excellent initial estimates and convergence was achieved after a few iterations with a fitting algorithm based on the Marquardt-Levenberg technique (see Press *et al.* 1992). The results are listed in Table 1. The orbit is circular within the measurement error. We therefore give the epoch of the passage of Aa through the ascending node, T_0, in the table.

The orbit is shown in Fig. 4. In the figure, a small arrow indicates the sense of revolution and T_0 denotes the ascending node. Two circles, one at the center and the other at the descending node, indicate the size of components Ab and Aa, respectively. Binary positions and corresponding uncertainty ellipses were derived from the data of each night in order to indicate the amount and quality of the data and their weights. The uncertainty ellipses were calculated as follows: we adopted the diameters and magnitude

differences from the global fit (see Table 1) and determined values for ρ and θ from the data of each night. (We accounted for orbital motion during the nights.) The visibility uncertainties were scaled to normalize the reduced χ^2 of the fit to unity, and uncertainty ellipses were fitted to the boundary of (ρ, θ) values, leading to an increase of the total χ^2 by one.

Table 2 lists the results; cols. 1 and 2 give date and fractional Besselian year of the observation (at 8 UT), col. 3 the length of the baseline, col. 4 the number of scans, cols. 5 and 6 separation and position angle (equinox 1991.9) at 8 UT, cols. 7 to 9 the axes and the position angle of the uncertainty ellipse, and col. 10 the deviation of the fitted binary position from the model values for ρ and θ. (Note that on November 12 and 13, 1992, baselines were switched *during* the night.) Position angles are measured counterclockwise from North.

4. COMPARISON OF DATA AND MODEL

The reduced χ^2 of the fit of the binary model (Table 1) to the visibility data is rather high: $\chi^2_\nu = 5.4$. However, this is probably due in part to an underestimation of the visibility uncertainties, because even for a fit on a single night (in which case there are more degrees of freedom available), the reduced χ^2 is significantly larger than unity (typically, $\chi^2_\nu \approx 2.5$). We note that, due to the enormous brightness of Capella, the photon-noise-induced uncertainty of the visibilities is often negligible compared with the calibration uncertainty. Thus, especially when the (squared) visibility is low, the estimated absolute uncertainty can be as small as 0.001. We have measured squared visibilities down to values of 0.005 and there is insufficient information on instrumental effects as to whether the visibilities should actually be assigned such a precision at such low levels of correlation (but see Quirrenbach *et al.* 1993). Ideally, one would like to have a check star in the vicinity of Capella with a similar brightness and degree of resolution, since the available calibrators are much fainter and unresolved. As for the estimation of the calibration uncertainty, we noted that on some occasions the seeing index of Capella scans covered

a range extending beyond that covered by calibrator scans. Again, this is due to the brightness of Capella, which enables the Mark III to track fringes even in inferior seeing conditions. Therefore, calibration of these scans is somewhat uncertain. This situation is related to the general question of transferability of the calibration from the calibrator stars to the program stars. For example, the determination of the time dependence of the normalization factor (see Sec. 2) might be somewhat affected by the specific position of the calibrators in the sky (see Mozurkewich *et al.* 1991 for the "Cassiopeia" effect). Applying such a calibration to the data of a program star might introduce systematic variations above the level of the estimated calibration uncertainty. We have, however, tried to minimize these effects by selecting calibrators close to the program stars.

Beyond the effect of underestimating the visibility uncertainties, there are inconsistencies between data and model, notably on the longest baselines, which indicate that the adopted binary model might not be entirely adequate. While model visibilities tend to be too low on baselines between 20 m and 24 m length (the latter being the longest one we used), they are too high (in the green channel) on the only two occasions on which we used an intermediate baseline of 15 m length. In Fig. 5, we show some of these data, taken during two consecutive nights in September 1992. On the second day, the baseline length is such that component Aa is measured very close to the first null of the visibility function. This means that any significant changes to the model visibility can only be accomplished by changing the diameter of Ab and/or its disk brightness distribution. We have fitted models to various subsets of data and found that it is only necessary to adjust the diameter of Ab to obtain a reasonable fit in every case. (Adjusting the diameter of Aa instead results in clearly inferior fits.) In view of the fact that Capella Ab is chromospherically active and our suspicion of RS CVn variability of this component (see Sec. 1), it is conceivable that star spot activity has affected the measured visibilities significantly. To simulate the effect of a single large spot of 40 degrees radius (angle subtended by the spot radius at the center of the star) with a local temperature 0.9 times the temperature

of the surrounding normal stellar surface, we used the Eclipsing Binary Computer Model (revision of 1992) by Wilson (1992, see also: Wilson 1979). This program calculates the stellar flux density on a grid spanning the visible hemispheres of the binary components, which can be used in a Fourier transformation to obtain the visibilities. By putting this spot on component Ab co-rotating at a latitude of 30 degrees south (assuming the visible pole to be the south pole and the rotational axis to coincide with the orbital angular momentum vector), we obtained the model visibilities as presented in Fig. 5 (dotted lines). This simple, yet reasonable model provides a significantly improved fit to the data. (We did not try to optimize the spot parameters in a systematic way. A spot of this size would lead to a brightness variation of Capella of about $0\overset{\mathrm{m}}{.}1$ peak-to-peak, not inconsistent with observations mentioned in the introduction.) However, true interferometric imaging is necessary to do a more detailed analysis of any deviations of the surface brightness distribution from a limb-darkened disk. We note that similar interferometric measurements close to and even beyond the first null of the visibility function led Di Benedetto & Bonneau (1990) to postulate small-scale structure on the surface of β Andromedae.

We show in Fig. 6 the normalized residuals between data and model, as well as the (formal) uncertainties of the visibilities. There is no systematic trend of the normalized residuals with visibility. The mean of the normalized residuals, however, is not zero, but has a small positive value. From simulations of data adopting a spotted disk for component Ab we found that this effect occurs when the standard limb-darkened binary model is fitted to this kind of data. In the event that strong star spot activity leads to significant offsets between the brightness center and the geometrical center of the disk, orbital elements might be influenced in a systematic way. Due to lack of information, we did not investigate this further. Instead, by using procedures described by Hummel *et al.* (1993), we performed Monte Carlo simulations of synthetic data sets (no spot activity assumed) in order to obtain realistic estimates for parameter uncertainties. For the uncertainties quoted in Table 1, we also took into account variations of the parameters

when fitting models to subsets of the observed data.

5. COMPARISON WITH PREVIOUS WORK

Our results for the orbital elements of Capella are in good agreement with, but (except for the period) more precise than the recent compilation by Barlow *et al.* (1993), which we list in Table 3. Barlow *et al.* had obtained new spectroscopic measurements and had calculated a combined solution from those and the speckle interferometric measurements collected in the *Second CHARA Catalog* (McAlister & Hartkopf 1988). They adopted a circular orbit, and we confirm the validity of this choice. Due to the relatively short time span the period is determined less accurately from our data than from the combined speckle and spectroscopic data. Both values agree within their uncertainties, and model parameters in a fit with the period taken from Barlow *et al.* (1993) are insignificantly different from the results listed in Table 1. We note, however, that our value for the major axis is larger than any of the previous determinations. This result is especially peculiar since quoted uncertainty estimates have usually been a small fraction of the discrepancy. It was in fact the first determination by Anderson (1920) which yielded the smallest value of $a = 52.5$ mas. Because of the high internal consistency of this first interferometric orbit, the results were included with high weight in subsequent investigations. Since then, however, estimates for the major axis were revised to ever larger values. We believe that there is in fact a scaling problem with the orbit of Anderson (1920) and Merrill (1922), which originates in their adoption of 550 nm as the effective wavelength of their visual measurements. This value was calibrated by observations of the Sun, and believed to be valid for observations of stars of spectral type G. However, the effective temperature of the Sun, $T_{\rm eff} = 5780$ K, is higher than the average temperature of the Capella stars, $T_{\rm eff} = 5310$ K (see below). The wavelength ratio of the spectral maxima Capella/Sun is 1.09; the ratio of the effective wavelengths resulting from a convolution of the spectra with the telescope-eye response curve will be somewhat closer to unity, but it is interesting to note that a ratio of 1.05 would account for magnitude and sign of the discrepancy in

the estimates for the major axis. It is unlikely that the cause of the scaling problem is related to the specific observational setup, since Kulagin (1970), using a visual periscopic interferometer but adopting the same effective wavelength, confirmed the earlier results.

We confirm the observation of Bagnuolo & Sowell (1988) that Capella Ab (the spectroscopic secondary) is the hotter component, and slightly brighter in the visual than Capella Aa. Our values for the magnitude difference are consistent with their results from speckle photometry, which are $\Delta m(y) = 0\overset{\mathrm{m}}{.}09$ and $\Delta m(b) = 0\overset{\mathrm{m}}{.}23$ for Strömgren filters y and b at $\lambda\lambda$ 547 nm and 467 nm, respectively. Similar results were obtained by Griffin & Griffin (1986; $\Delta m_{\mathrm{V}} = 0\overset{\mathrm{m}}{.}15$) and Strassmeier & Fekel (1990; $\Delta m_{643\,\mathrm{nm}} = 0\overset{\mathrm{m}}{.}08$) using spectrophotometry. We also confirm the diameter of 6.3 mas measured for Capella Ab by Di Benedetto & Bonneau (1991) in the infrared.

5. DISCUSSION

It is not only from the determination of accurate stellar masses that interferometric double star observations derive their importance. The ability to measure the diameters and magnitude difference of the components allows the direct determination of the luminosities and effective temperatures, if additional information on the total bolometric flux is available. Masses, luminosities and effective temperatures are basic parameters to be compared with the predictions of stellar evolution models. An important addition to the measured quantities of the Capella system is our diameter of component Aa and the confirmation of the Ab diameter measured by Di Benedetto & Bonneau (1991).

5.1 Distance, Absolute Magnitudes, and Colors

For circular orbits, $D = 0.09192(K_1 + K_2)P(\sin i)^{-1}a^{-1}$ pc, which gives a distance of $D = (13.3 \pm 0.1)$ pc to Capella, corresponding to a distance modulus of $0\overset{\mathrm{m}}{.}62 \pm 0\overset{\mathrm{m}}{.}01$. The orbital parallax is $\pi_{\mathrm{orb}} = 0\overset{''}{.}0751 \pm 0\overset{''}{.}0005$, in excellent agreement with the trigonometric parallax $\pi = 0\overset{''}{.}076 \pm 0\overset{''}{.}003$ determined by Heintz (1975). At this small a distance, interstellar absorption and reddening will have no noticeable effect on our results.

With the magnitude differences and the distance measured, we calculated absolute magnitudes $M_{\rm Aa,Ab}$ at $I_{\rm C}$, V, and B for each component, using the apparent combined magnitudes, $m_{\rm Aa+Ab}$, given by Johnson *et al.* (1966) in the $UBVRI$ system. (We used the formula given by Bessell (1979) to convert $(V - I_{\rm J})$ to $(V - I_{\rm C})$. The Cousins I-band at 789 nm is close to our 800 nm band.) We adopted independent uncertainties in the B, V, and $I_{\rm C}$ bands of $0\overset{\rm m}{.}03$. Table 4 lists the results. We then derived $(B - V)$ colors of $0\overset{\rm m}{.}74 \pm 0\overset{\rm m}{.}07$ for for component Ab and $0\overset{\rm m}{.}87 \pm 0\overset{\rm m}{.}08$ for Aa. Within the uncertainty, these colors are consistent with classifications G1III and G8III determined by Strassmeier & Fekel (1990) for components Ab and Aa, for which Flower (1977) gives $(B - V) = 0\overset{\rm m}{.}70$ and $(B - V) \approx 0\overset{\rm m}{.}92$, respectively. A word of caution is in order, however, since our filter bandpasses do not correspond exactly to the Johnson filters, especially in regard to their widths.

5.2 Effective Temperatures and Luminosities

The measurement of the diameters allows us to derive a direct estimate of the stellar effective temperatures, provided we obtain the bolometric corrections. Gubochkin & Miroshnichenko (1991) have used the surface-brightness method to derive the bolometric correction as a function of the effective temperature. We use their formula (6), $BC = -0.0508T_3^2 + 0.762T_3 - 2.831\,(4.7 < T_3 < 10;\, T_3 \equiv T_{\rm eff}/1000{\rm K})$, and the relations $1.13 \cdot 10^{15} L/L_\odot = (R/R_\odot)^2 T_{\rm eff}^4$ and $M_{\rm bol} \equiv M_V - BC = -2.5\log(L/L_\odot) + 4\overset{\rm m}{.}72$ to determine both effective temperatures and bolometric luminosities by way of iteration. The results are listed in Table 5. Again, the effective temperatures are consistent with the spectral classifications.

We obtain an independent confirmation of the derived luminosities by integrating the combined ultraviolet–infrared energy distribution of the Capella stars. We used measurements by Thompson *et al.* (1978) in the UV at 156.5 nm, 196.5 nm, 236.5 nm, and 274.0 nm, by Glushneva *et al.* (1992) in the range 320 nm – 1080 nm in 5-nm intervals, by Johnson *et al.* (1966) in the UBVRIJKL bands (using the absolute calibration

by Johnson 1965), and by the IRAS satellite at 12μm, 25μm, 60μm, and 100μm. Flux contribution from outside this range is negligible. The resulting total bolometric luminosity, $L_{Aa+Ab}/L_\odot = 153$, agrees with the values given in Table 5 at the 2 percent level, corresponding to an error in the bolometric correction of only $0\overset{\mathrm{m}}{.}02$.

5.3 Stellar Masses and Comparison with Evolutionary Models

For circular orbits, $\mathcal{M}_{1,2} = 1.0385 \cdot 10^{-7}(K_1 + K_2)^2 K_{2,1} P (\sin i)^{-3}\ \mathcal{M}_\odot$, which gives $\mathcal{M}_{\rm Aa} = (2.69 \pm 0.06)\mathcal{M}_\odot$ and $\mathcal{M}_{\rm Ab} = (2.56 \pm 0.04)\mathcal{M}_\odot$. We now have the necessary information to determine the evolutionary state of the Capella system. For this purpose, we use the stellar evolution models published by Schaller *et al.* (1992) and Schaerer *et al.* (1993) for metallicities $Z = 0.001$, 0.008, and 0.020. (The tables, as well as a program to construct isochrones, were kindly made available to us by G. Meynet.) We need to find a coeval stellar pair with predicted values for masses, temperatures and luminosities consistent with the measurements. Such a pair exists on the $Z = 0.008$ isochrone for $\log(age/\mathrm{y}) = 8.720$, with masses of 2.51 $\mathcal{M}_\odot$ and 2.54 $\mathcal{M}_\odot$ for components Ab and Aa, respectively (mass ratio 1.013). In this scenario, the primary has undergone helium ignition. The model is shown in Fig. 7. The masses are slightly too low, and a better model may be found by increasing the metallicity somewhat. Adoption of the $Z = 0.008$ isochrone is supported by the measurements of McWilliam (1990), who obtained $Z = 0.009$. In addition, if we want the model to reproduce the spectroscopically determined mass ratio which is significantly different from unity (see next paragraph), solar metallicity models are ruled out since they assign both components to the same, i.e. pre-helium ignition phase on the isochrone.

As can be seen from Fig. 7, the luminosity and temperature of component Aa alone unfortunately provide insufficient information on whether or not this component has undergone helium ignition. It is essentially the mass ratio, q (notoriously difficult to determine from spectroscopy for Capella due to the rotationally broadened lines of Ab), which distinguishes the two scenarios. The mass ratio has to be very close to unity if the

components are to be in similar phases close to the end of hydrogen fusion. Wright (1954) determined $q = 1.04 \pm 0.03$, Shen *et al.* (1985) $q = 1.18 \pm 0.02$, Batten *et al.* (1991) $q = 1.025 \pm 0.028$, and Barlow *et al.* (1993) $q = 1.052 \pm 0.012$. Thus, it seems helium ignition must have taken place in Aa. This conclusion was supported by Pilachowski & Sowell (1992) based on the observation of a low lithium abundance in Aa, which is expected to occur when the stellar envelope becomes fully convective. Further evidence in support of this scenario is the extremely low limit on the eccentricity of the orbit, and a discussion of orbital circularization can be found in Barlow *et al.* (1993) and Andersen *et al.* (1991).

We thank Lu Rarogiewicz and Craig Denison for their most helpful assistance in operating the Mark III interferometer for many years. This work was supported by the Office of Naval Research. A. Q. is supported by the Alexander von Humboldt foundation through a Feodor Lynen fellowship. This research has made use of the SIMBAD literature database, operated at CDS, Strasbourg, France.

References

Andersen, J., Clausen, J. V., Nordström, B., Tomkin, J., & Mayor, M. 1991, A&A, 246, 99

Anderson, J. A. 1920, ApJ, 51, 263

Armstrong, J. T., Mozurkewich, D., Vivekanand, M., Simon, R. S., Denison, C. S., Johnston, K. J., Pan, X.-P., Shao, M., & Colavita, M. M. 1992, AJ, 104, 241

Ayres, T. R., & Linsky, J. L. 1980, ApJ, 241, 279

Bagnuolo, W. G., & Hartkopf, W. I. 1989, AJ, 98, 2275

Bagnuolo, W. G., & Sowell, J. R. 1988, AJ, 96, 1056

Barlow, D. J., Fekel, F. C., & Scarfe, C. D. 1993, PASP, 105, 476

Batten, A. H., Fletcher, J. M., & MacCarthy, D. G. 1989, Pub. Dom. Astrophys. Obs., 17, 1

Batten, A. H., Hill, G., Lu, W. 1991, PASP, 103, 623

Bessell, M. S. 1979, PASP, 91, 589

Di Benedetto, G. P., & Bonneau, D. 1990, ApJ, 358, 617

Di Benedetto, G. P., & Bonneau, D. 1991, A&A, 252, 645

Fekel, F. C., Moffett, T. J., & Henry, G. W. 1986, ApJS, 60, 551

Flower, P. J. 1977, A&A, 54, 31

Glushneva, I. N., Kharitonov, A. V., Knyazeva, L. N., & Shenavrin, V. I. 1992, A&AS, 92, 1

Griffin, R., & Griffin, R. 1986, J. Astrophys. Astron., 7, 45

Gubochkin, A. N., Miroshnichenko, A. S. 1991, Kin. and Phys. of Cel. Bodies, 7, 59

Hall, D. S. 1981, in: Solar Phenomena in Stars and Stellar Systems, edited by R. M. Bonnet and A. K. Dupree (Reidel, Dordrecht), p. 431

Hanbury Brown, R., Davis, J., Lake, R. J. W., & Thompson, R. J. 1974, MNRAS, 167, 475

Heintz, W. D. 1975, ApJ, 195, 411

Hoffleit, D., & Jaschek, C. 1982, The Bright Star Catalogue (Yale University Observatory, New Haven)

Hummel, C. A., & Armstrong, J. T. 1993, in Very High Angular Resolution Imaging, IAU Symposium No. 158 (preprint)

Hummel, C. A., Armstrong, J. T., Quirrenbach, A., Buscher, D. F., Mozurkewich, D., Simon, R. S., & Johnston, K. J. 1993, AJ, 106, 2486

Johnson, H. L. 1965, Comm. Lunar Planetary Lab., 3, 73

Johnson, H. L., Mitchell, R. I., Iriarte, B., & Wiśniewski, W. Z. 1966, Comm. Lunar Planetary Lab., 4, 99

Krisciunas, K., & Guinan, E. 1990, IAU Inform. Bull. Var. Stars, 3548, 1

Kukarkin, B. V., Kholopov, P. N., Artiukhina, N. M., Fedorovich, V. P., Frolov, M. S., Goranskij, V. P., Gorynya, N. A., Karitskaya, E. A., Kireeva, N. N., Kurkakina, N. P., Kurochkin, N. E., Medvedeva, G. I., Perova, N. B., Ponomareva, G. A., Samus', N. N., Shugarov, S. Yu. 1982, New Catalogue of Suspected Variable Stars (Nauka, Moscow)

Kulagin, E. S. 1970, Astron. Zh., 47, 557 [Sov. Astron.–AJ 1970, 14, 445]

Manduca, A. 1979, A&AS, 36, 411

Manduca, A., Bell, R. A., & Gustafsson, B. 1977, A&A, 61, 809

McAlister, H. A. 1981, AJ, 86, 795

McAlister, H. A., & Hartkopf, W. I. 1988, Second Catalog of Interferometric Observations of Binary Stars (CHARA Contribution No. 2, Georgia State University, Atlanta)

McWilliam, A. 1990, ApJS, 74, 1075

Merrill, P. W. 1922, ApJ, 56, 40

Mozurkewich, D., Johnston, K. J., Simon, R. S., Bowers, P. F., Gaume, R. A., Hutter, D. J., Colavita, M. M., Shao, M., & Pan, X.P. 1991, AJ, 101, 2207

Petit, M. 1990, A&AS, 85, 971

Pilachowski, C. A., & Sowell, J. R. 1992, AJ, 103, 1668

Press, W. H., Flannery, B. P., Teukolsky, S. A., & Vetterling, W. T. 1992, Numerical Recipes (Cambridge University Press, Cambridge)

Quirrenbach, A. *et al.* 1993, in Very High Angular Resolution Imaging, IAU Symposium No. 158 (preprint)

Schaerer, D., Meynet, G., Maeder, A., & Schaller, G. 1993, A&AS, 98, 523

Schaller, G., Schaerer, D., Meynet, G., & Maeder, A. 1992, A&AS, 96, 269

Shao, M., Colavita, M. M., Hines, B. E., Staelin, D. H., Hutter, D. J., Johnston, K. J., Mozurkewich, D., Simon, R. S., Hershey, J. L., Hughes, J. A., & Kaplan, G. H. 1988, A&A, 193, 357

Shen, L.-Z., Beavers, W. I., Eitter, J. J., & Salzer, J. J. 1985, AJ, 90, 1503

Strassmeier, K. G., & Fekel, F. C. 1990, A&A, 230, 389

Thompson, G. I., Nandy, K., Jamar, C. Monfils, A., Houziaux, L., Carnochan, D. J., & Wilson, R. 1978, Catalogue of Stellar UV Fluxes, Science Research Council, UK

Wilson, R. E. 1979, ApJ, 234, 1054

Wilson, R. E. 1992, in: New Frontiers in Interacting Binary Star Research, eds. J. C. Leung and I.-S. Nha (ASP Conference Series, San Francisco), p. 91

Wright, K. O. 1954, Publ. Dom. Astrophys. Obs., 10, 1; ApJ, 119, 471

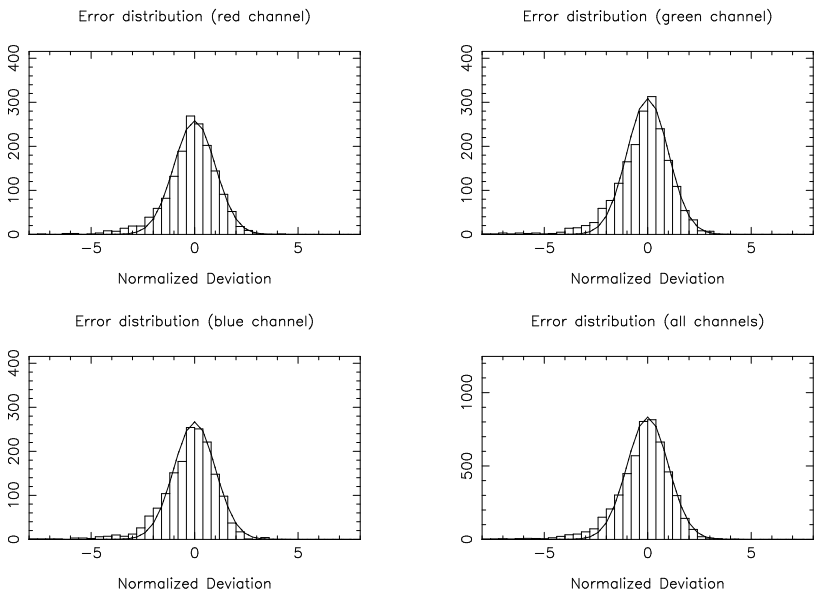

Figure 1: Visibility error histograms for the calibrators. The solid curves indicate Gaussian distributions for $\chi^2_\nu = 1$.

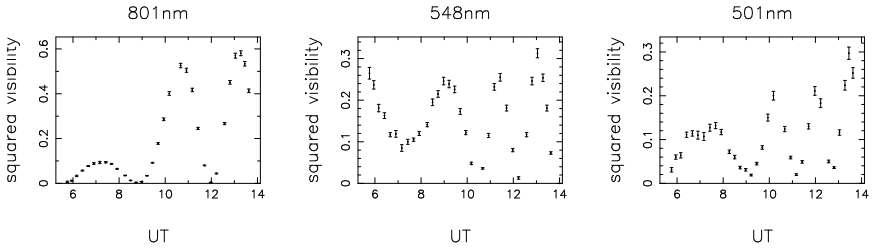

Figure 2: Squared visibility of Capella versus UT on November 13, 1991.

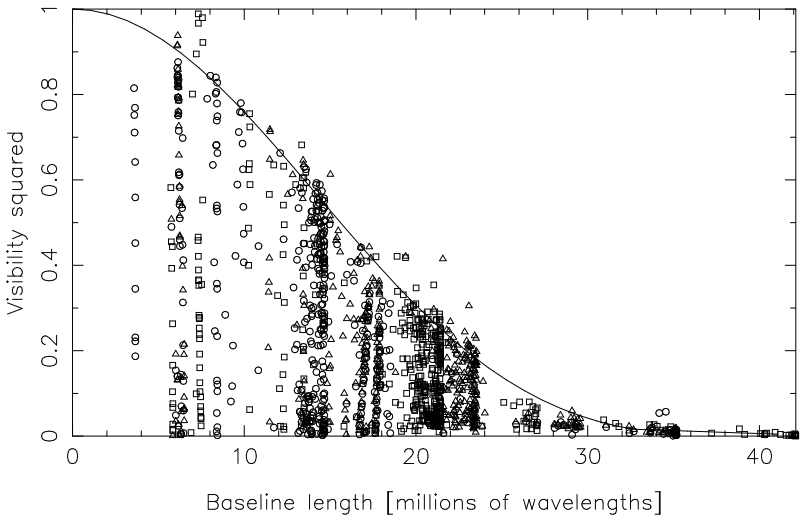

Figure 3: All measured visibility amplitudes plotted versus the (projected) baseline length. Open circles denote data of the red channels, open squares data of the green channels, open triangles data of the blue channels. Solid line indicates upper envelope of visibilities calculated for a model at 500 nm.

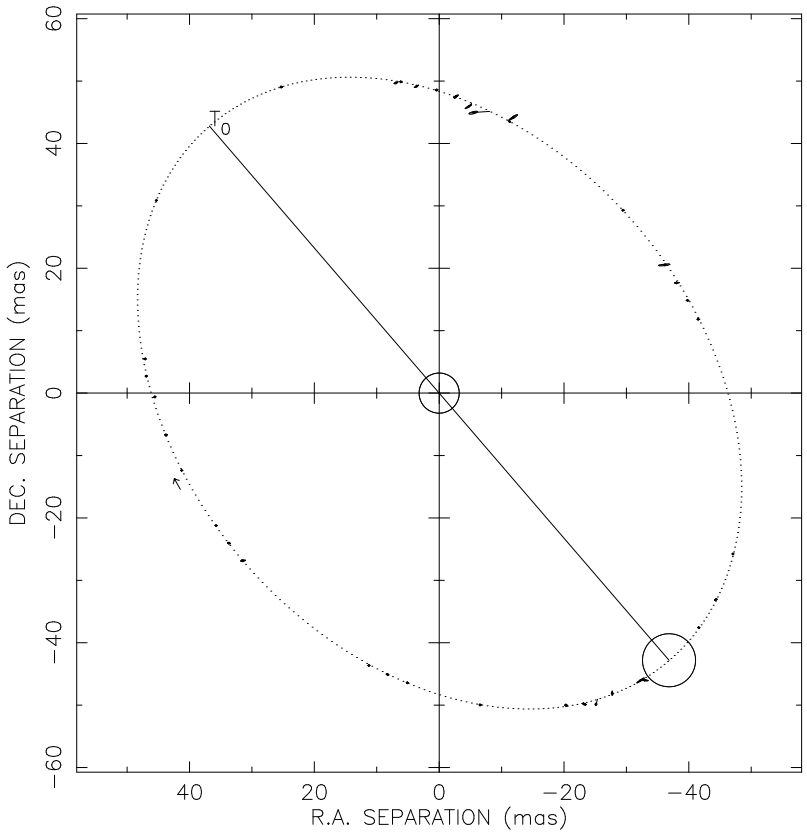

Figure 4: The apparent orbit of Capella.

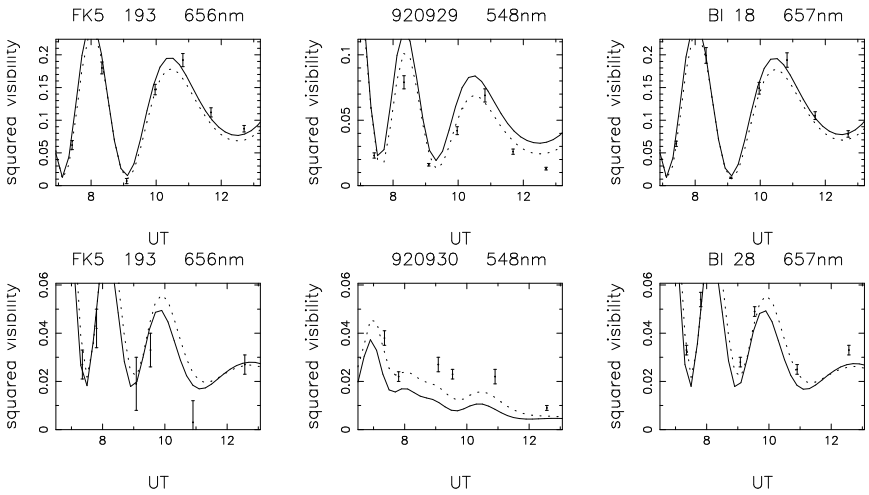

Figure 5: Visibilities for the model of Table 1 (solid line) and a model featuring a star spot on the disk of Capella Ab (dotted line), plotted together with observed data. Dates: YYMMDD.

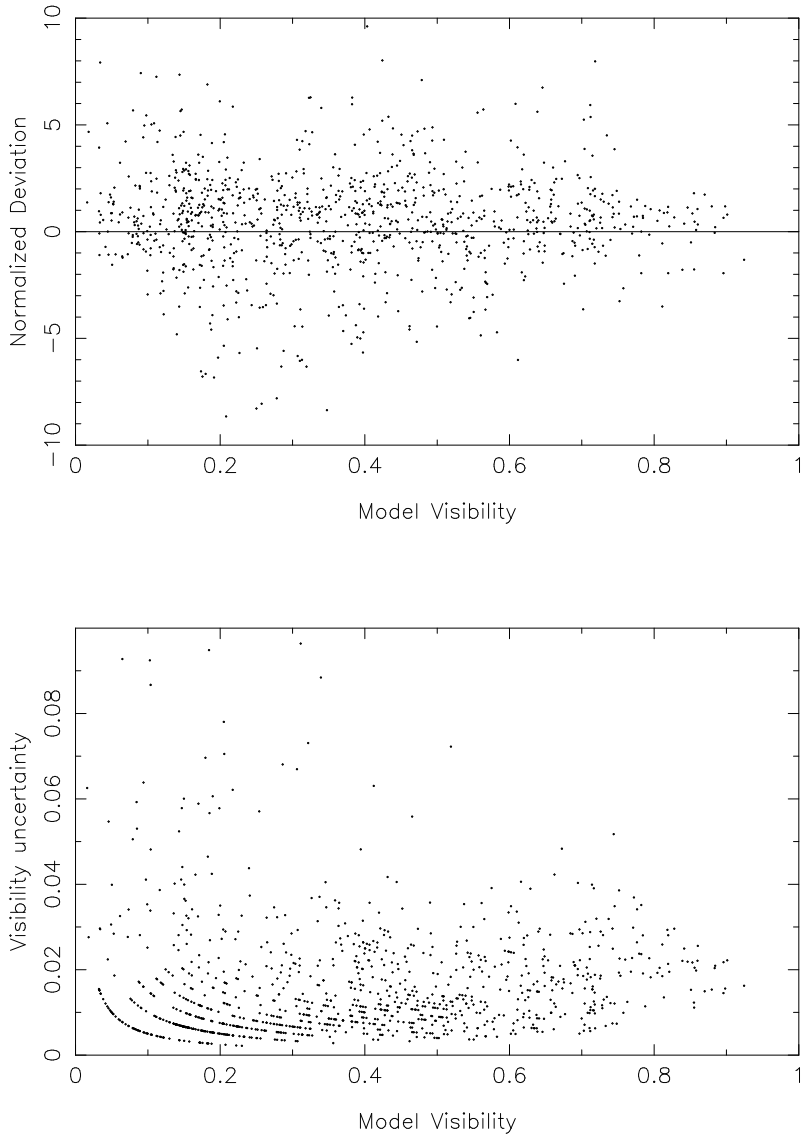

Figure 6: Normalized residuals (i.e. the deviation of the measured visibility from the model visibility, divided by the formal uncertainty of the measured visibility), and (formal) visibility uncertainties, plotted versus the model visibility. (The grouping of the points into lines in the lower plot is due to a floating point number representation with insufficient precision.)

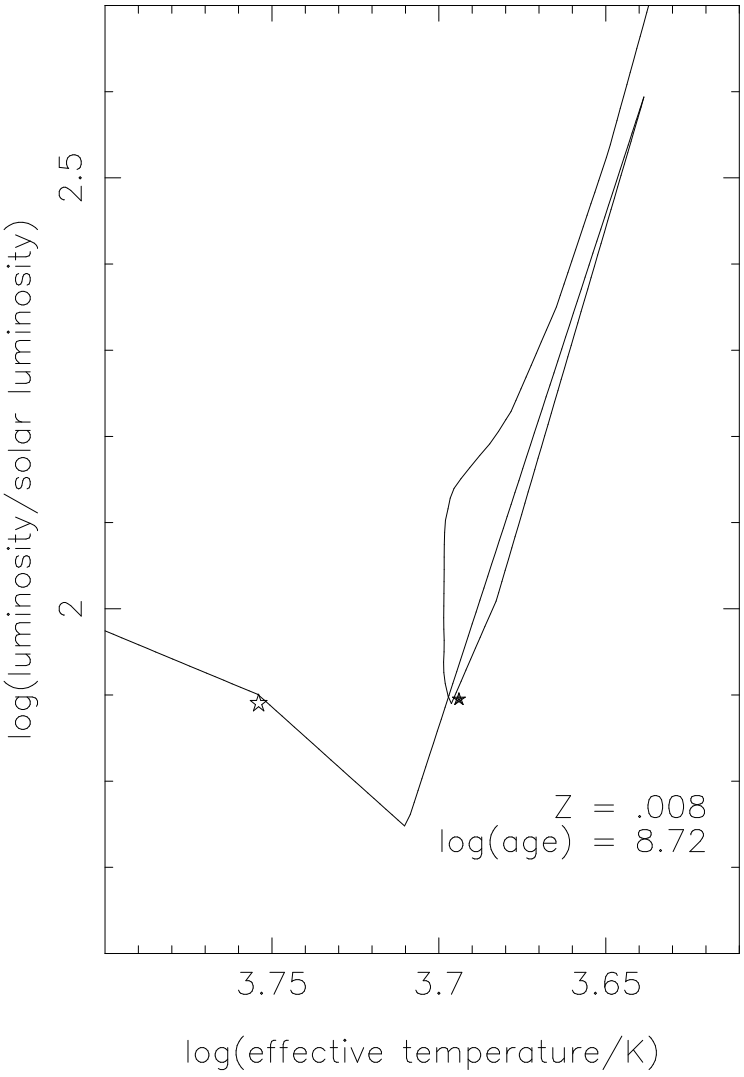

Figure 7: Evolutionary state of the Capella stars. The open star symbol denotes component Ab. Solid curve is isochrone.

TABLE 1. Orbital elements and component parameters from the Mark III interferometer.

Parameter	value	uncertainty
a/mas	56.47	0.05
e	0.0000	0.0002
i	$137\overset{\circ}{.}18$	$0\overset{\circ}{.}05$
Ω (2000.0)	$40\overset{\circ}{.}8$	$0\overset{\circ}{.}1$
T_0	JD2447528.45	0.02
P/days	104.022	0.002
D_1/mas	6.4	0.3
D_2/mas	8.5	0.1
$\Delta m_{800\mathrm{nm}}$	$-0\overset{\mathrm{m}}{.}05$	$0\overset{\mathrm{m}}{.}05$
$\Delta m_{550\mathrm{nm}}$	$+0\overset{\mathrm{m}}{.}15$	$0\overset{\mathrm{m}}{.}05$
$\Delta m_{450\mathrm{nm}}$	$+0\overset{\mathrm{m}}{.}28$	$0\overset{\mathrm{m}}{.}10$
Note:	$\Delta m \equiv m_{\mathrm{Aa}} - m_{\mathrm{Ab}}$	

TABLE 2. Observation and result log for Capella.

UT Date (1)	Bess. Yr. (+1900) (2)	BL [m] (3)	No. scans (4)	ρ [mas] (5)	θ [deg] (6)	$\sigma_{\rm maj}$ [mas] (7)	$\sigma_{\rm min}$ [mas] (8)	φ [deg] (9)	O-C [mas] (10)
1988									
Oct 18	88.7973	3.0	6	41.61	299.60	0.95	0.11	96.3	0.21
Oct 19	88.8000	3.0	6	41.95	294.92	0.42	0.03	93.3	0.21
Oct 20	88.8028	5.3	9	42.50	290.45	0.22	0.03	85.7	0.15
Oct 21	88.8055	6.9	13	43.14	285.92	0.15	0.02	88.2	0.07
1990									
Dec 10	90.9411	12.0	9	43.09	106.71	0.09	0.02	86.6	0.04
Dec 15	90.9548	12.0	6	47.02	86.69	0.13	0.05	88.6	0.09
1991									
Sep 19	91.7159	12.0	4	56.22	215.02	0.73	0.08	124.1	0.15
Sep 21	91.7214	12.0	5	55.52	209.97	0.37	0.06	179.6	0.13
Sep 22	91.7241	12.0	6	55.83	206.75	0.23	0.05	156.5	0.85
Oct 15	91.7871	6.9	15	41.58	120.69	0.07	0.01	93.7	0.19
Nov 2	91.8364	15.2	15	54.84	55.74	0.07	0.02	91.6	0.08
Nov 13	91.8665	11.4	32	55.19	27.31	0.04	0.01	94.5	0.09
Nov 20	91.8857	12.0	12	50.26	7.04	0.06	0.02	88.4	0.11
Nov 23	91.8939	12.0	12	47.43	357.00	0.10	0.05	149.3	0.13
Nov 26	91.9021	12.0	9	44.95	345.45	0.16	0.05	77.9	0.15
Dec 22	91.9733	12.0	11	53.67	241.29	0.10	0.03	87.6	0.03
Dec 27	91.9870	11.4	13	56.04	227.91	0.09	0.02	77.5	0.07
1992									
Jan 1	92.0006	23.6	13	56.55	215.58	0.50	0.07	83.0	0.46
Jan 16	92.0417	12.0	7	45.84	169.60	0.24	0.05	73.4	0.04
Jan 17	92.0445	12.0	10	45.07	165.52	0.09	0.02	83.8	0.16
Jan 26	92.0691	12.0	6	41.39	125.52	0.25	0.05	74.6	0.20
Feb 1	92.0855	12.0	7	44.28	98.69	0.22	0.02	93.5	0.18
Feb 5	92.0965	12.0	11	47.41	83.36	0.10	0.02	78.5	0.44
Sep 27	92.7399	4.3	5	50.18	7.95	0.33	0.05	111.1	0.52
Sep 28	92.7426	11.4	4	49.31	4.18	0.42	0.04	118.5	0.13
Sep 29	92.7454	15.2	7	48.56	0.48	0.21	0.06	110.6	0.23
Sep 30	92.7481	19.7	6	47.62	356.74	0.40	0.09	121.2	0.42
Oct 1	92.7508	19.7	6	46.16	354.13	0.62	0.08	121.3	0.70
Oct 2	92.7536	23.6	6	45.30	352.99	0.71	0.16	103.9	2.58
Oct 3	92.7563	23.6	6	45.81	344.90	0.76	0.12	121.9	1.12
Oct 10	92.7755	12.0	23	41.53	314.87	0.05	0.01	105.9	0.09
Nov 1	92.8357	12.0	13	55.32	233.29	0.19	0.02	118.1	0.05
Nov 12	92.8658	12.0	15	54.89	204.93	0.09	0.04	78.1	0.13
Nov 12	92.8658	4.3	11	55.11	205.13	0.14	0.04	91.8	0.41
Nov 13	92.8686	12.0	51	54.04	202.18	0.09	0.02	69.5	0.13
Nov 13	92.8686	4.3	18	53.96	202.09	0.14	0.07	92.9	0.23
Nov 18	92.8823	12.0	23	50.39	187.46	0.07	0.02	88.8	0.07
Nov 22	92.8932	8.2	13	46.68	173.71	0.11	0.02	116.4	0.07
Dec 2	92.9206	12.0	6	41.36	130.48	0.43	0.07	98.8	0.14
Dec 11	92.9452	12.0	8	45.55	90.75	0.15	0.03	113.0	0.47

TABLE 3. Orbital elements from spectroscopy and speckle interferometry (Barlow *et al.* 1993).

a	55.7±0.3 mas
i	$136\overset{\circ}{.}7 \pm 0\overset{\circ}{.}4$
Ω	$40\overset{\circ}{.}9 \pm 0\overset{\circ}{.}3$
T_0	JD 2442119.249 ± 0.077 days
P	104.0233 ± 0.0008 days
K_1	26.05±0.10 km/s
K_2	27.40±0.30 km/s
Note:	52 orbital periods added to T_0 give T_0 = 2447528.461.

TABLE 4. Limb-darkening coefficients A and magnitudes.

	Band, effective wavelength [nm]		
	$I_{\rm C}$	V	B
	800	550	450
$A^a_{\rm Aa}$	0.540	0.749	0.885
$A^a_{\rm Ab}$	0.476	0.681	0.804
$M_{\rm Aa}$	$-0\overset{\rm m}{.}62 \pm 0\overset{\rm m}{.}04$	$0\overset{\rm m}{.}29 \pm 0\overset{\rm m}{.}04$	$1\overset{\rm m}{.}16 \pm 0\overset{\rm m}{.}05$
$M_{\rm Ab}$	$-0\overset{\rm m}{.}57 \pm 0\overset{\rm m}{.}04$	$0\overset{\rm m}{.}14 \pm 0\overset{\rm m}{.}04$	$0\overset{\rm m}{.}88 \pm 0\overset{\rm m}{.}05$
$m^b_{\rm Aa+Ab}$	$-0\overset{\rm m}{.}73$	$0\overset{\rm m}{.}08$	$0\overset{\rm m}{.}88$

[a] Limb-darkening coefficients (adopted, see Sec. 3)
[b] Johnson *et al.* (1966)

TABLE 5. Physical parameters of the Capella stars.

Parameter	Ab	Aa
Mass/$\mathcal{M}_\odot$	2.56 ± 0.04	2.69 ± 0.06
Luminosity/$L_\odot$	77.6 ± 2.6	78.5 ± 1.2
$T_{\rm eff}$/K	5700 ± 100	4940 ± 50
$(B-V)$	$0\overset{\rm m}{.}74 \pm 0\overset{\rm m}{.}07$	$0\overset{\rm m}{.}87 \pm 0\overset{\rm m}{.}08$
$(V-I)_{\rm C}$	$0\overset{\rm m}{.}71 \pm 0\overset{\rm m}{.}05$	$0\overset{\rm m}{.}91 \pm 0\overset{\rm m}{.}06$
Radius/$R_\odot$	9.2 ± 0.4	12.2 ± 0.2